## Direct measurement of $\pi$ coupling at the single molecule level using a carbon nanotube force sensor

Tu  $Hong^1$ , Tianjiao  $Wang^1$ , and Ya-Qiong  $Xu^{1,2,*}$ 

<sup>1</sup>Department of Electrical Engineering and Computer Science, <sup>2</sup>Department of Physics and Astronomy, Vanderbilt University, Nashville, TN 37212, USA

<sup>\*</sup>Correspondence to: <u>yaqiong.xu@vanderbilt.edu</u>

**ABSTRACT** 

We report a carbon nanotube (CNT) force sensor that combines a suspended CNT transistor with

dual-trap optical tweezers to explore the interactions between two individual molecules in the near-

equilibrium regime with sub-piconewton resolution. The directly-measured equilibrium force (1.2)

 $\pm$  0.5 pN) is likely related to the binding force between a CNT and a single DNA base, where two

aromatic rings spontaneously attract to each other due to the noncovalent forces between them.

Based on our force measurements, the binding free energy per base is calculated (~ 0.34 eV),

which is in good agreement with theoretical simulations. Moreover, three-dimensional scanning

photocurrent microscopy enables us to simultaneously monitor the morphology changes of the

CNT, leading to a comprehensive reconstruction of the CNT-DNA binding dynamics. These

experimental results shed light on the fundamental understanding of the mechanical coupling

between CNTs and DNA molecules and more importantly, provide a new platform for direct

observation of intermolecular interface at the single-molecule level.

**Keywords:** carbon nanotube, DNA, photocurrent, optical trapping, transistors

2

Interactions between  $\pi$ -electron systems are abundant in nature and these non-covalent bindings play fundamental roles in a wide variety of disciplines, such as physics, chemistry, biology, materials science, and nanotechnology. Numerous efforts have been made to investigate these interactions using isothermal titration calorimetry, conformational isomerism, and chemical double mutant cycle, and direct force measurements. Nhile providing valuable information on the binding strength of  $\pi$  coupling, these methods depend on the averaging of ensemble data and oversimplifies the fluctuating details from single-aromatic ring interactions that are essential to the fundamental understanding of the interfaces in  $\pi$ -electron systems. Therefore, a complete understanding of these nanoscale interactions is still missing, owing to the lack of experimental detection of  $\pi$  coupling at the single molecule level in the near-equilibrium regime. Measuring the binding force between two individual aromatic rings has been extremely challenging due to limited instrumental spatial resolution, in terms of both physical dimensions of probes and the ability to control objects with single-molecule precision.

CNTs are one-dimensional materials with exceptional electrical, optical, thermal, and mechanical properties. <sup>17-21</sup> Their diameters can easily achieve sub-1-nm scale, providing a natural platform for binding of single aromatic ring structures. Field effect transistors (FETs) based on CNTs have been studied to identify single-molecule dynamics through conductance measurements with molecules that bind to defect sites on CNTs<sup>22</sup> or attach through noncovalent mobilization. <sup>22</sup>, However, precise control of the binding molecules on CNT sidewalls remains unsolved. Optical tweezers are promising tools for micromanipulation of single biological molecules, offering precise three-dimensional manipulation of trapped objects with sub-piconewton force measurement accuracy and sub-millisecond temporal resolution. <sup>24-26</sup>

Here, by taking advantage of the intrinsic small diameter of a carbon nanotube (CNT), we report a CNT force sensor that combines a suspended CNT transistor with dual-trap optical tweezers to explore the interactions between two individual molecules in the near-equilibrium regime with sub-piconewton resolution. The directly-measured equilibrium force  $(1.2 \pm 0.5 \text{ pN})$  is likely related to the binding force between a CNT and a single DNA base, where two aromatic rings spontaneously attract to each other due to the noncovalent forces between them. Based on our force measurements, the binding free energy per base is calculated ( $\sim 0.34 \text{ eV}$ ), which is in good agreement with theoretical simulations.<sup>27-36</sup> Moreover, three-dimensional scanning photocurrent microscopy enables us to simultaneously monitor the morphology changes of the CNT transistor<sup>37-39</sup> to reconstruct the CNT-DNA binding dynamics. These experimental results are the first direct measurement of the binding force between two individual aromatic rings, which not only provide an in-depth understanding of the ubiquitous interactions but also offer an ultrasensitive probing platform to explore the mechanical coupling of the nano-bio interfaces at the single-molecule level.

We fabricated Pt electrodes separated by a 5  $\mu$ m wide and 4  $\mu$ m deep trench on a 170  $\mu$ m thick transparent fused silica substrate. CNTs, which suspended over the trench, were subsequently synthesized by chemical vapor deposition to connect the two electrodes (Fig. 1a). Direct growth of CNTs allows for ultraclean carbon surfaces without contamination, minimizing the undesirable influence during the fabrication processes. We then chose CNT FETs in which only one nanotube bridged two electrodes for further experiments (Fig. 1b). Next, the CNT transistor was sealed in a microfluidic chamber with a large gold pad that acted as an electrolyte gate to modulate the electrochemical environment of the CNT. Gate-dependent conductance measurement of a typical

CNT transistor displays p-type semiconducting characteristics, consistent with previous reports of electrolyte-gated CNT transistors. 40,41

High-resolution dual-trap optical tweezers ( $\lambda = 1064 \text{ nm})^{37, 42}$  were adapted into our optoelectronic probing system to manipulate a single double-stranded DNA (dsDNA) molecule ( $\sim$  5 kbp). The dsDNA molecule was end-modified and attached to a microscopic polystyrene bead on each end to form a dsDNA tether (Fig. S1a). The distance between the beads was controlled by moving two optical traps through two piezo-controlled rotary mirrors, respectively. We further combined dual-trap optical tweezers with a 3D scanning photocurrent microscopy setup to allow simultaneous recording of photo-generated current signals and reflection light of a CNT transistor when another laser beam ( $\lambda = 785 \text{ nm}$ ) spatially scanned over the CNT. This technique not only probes local optoelectronic properties of the CNT, but also offers information of its position and morphology. By overlapping optical and photocurrent images of a CNT transistor (Fig. 1c), we can precisely locate the CNT position relative to the dsDNA tether. Figure 1d shows the scanning photocurrent image of a CNT transistor in the *xy* plane, with coordinates defined in Fig. 1a. The photocurrent responses originate from electron-hole pair separation due to Schottky barriers at electrode-CNT junctions and local band-bending along the CNT.<sup>37, 38</sup>

The behaviors of dsDNA and single-stranded DNA (ssDNA) are significantly different when they attach to the surface of CNTs. Typically, the binding force between ssDNA and CNTs is relatively strong due to the interactions between DNA bases and the hexagonal lattice of CNT sidewalls, <sup>2, 43-45</sup> whereas the hydrophilic backbone of dsDNA are not spontaneously attracted to the uncharged surface of CNTs. <sup>46</sup> We first investigate the binding between CNTs and ssDNA. Here, ssDNA segments were randomly generated by overstretching a dsDNA tether, and some of these segments could locate in the middle of the DNA tether <sup>47, 48</sup> (supplementary information).

The creation of the ssDNA-dsDNA hybrid was confirmed by the force-extension curve of the DNA that was noticeably different from the elastic behavior of a dsDNA (Fig. S2b).<sup>47, 49</sup> In comparison with ssDNA, this hybrid DNA structure partially maintains the rigidity of dsDNA and can generally avoid the floppiness and complicated secondary structures of typical ssDNA molecules.

We determine the force applied to the hybrid DNA by video image analysis (VIA) of bead displacements in the lateral and axial directions, respectively.<sup>37, 50</sup> Figure 2a shows the experimental geometry in the xz plane. The distance between the optical trap center and bead center in the x and z directions are defined as  $x_{bead}$  and  $z_{bead}$ , respectively. We only considered the right optical trap here since similar results were obtained from the left optical trap. The forces applied to the beads by optical tweezers were calculated based on bead displacements from VIA and trap stiffness obtained from position sensitive detectors (PSDs) (supplementary information). We also used PSDs to collect transmitted laser beams to calculate the force applied to the hybrid DNA in the lateral direction to further verify our VIA results, while PSD measurements are insufficient to determine the force in the axial direction. In our experiments, we moved the hybrid DNA tether to the area above the suspended CNT. The middle of the hybrid DNA tether was placed atop the center of the CNT in the perpendicular direction (Fig. 1a) so the forces applied to the left and the right bead were almost symmetric when the DNA molecule was attached to the CNT. To minimize the friction forces induced by parallel sliding, we focused on the force measurements in which the forces on the left and right beads were balanced. Therefore, the majority of the external force applied in the direction normal to the molecular plane and our measured force is expected to be the adhesive force between a CNT and DNA molecule. Typical forces applied on a bead by optical traps are shown in Fig. 2b. The green curve represents the z position of the optical trap centers relative to the electrode plane. When the hybrid DNA tether was pushed down by optical traps in

the direction toward the CNT, the force remained constant ( $F_z = 0$ , blue) until the DNA tether touched the CNT surface (z = 0), where the electrodes, CNT, optical trap centers, and bead centers lied roughly in the same plane. Subsequently, the force in the axial direction ( $|F_z|$ ) started to increase when the optical traps were further moved down, indicating that the DNA tether pushed the CNT down while the CNT held up the DNA tether and dragged the beads away from the optical trap centers. As a result, a force towards the center of the optical trap was applied to the bead, leading to force changes in both negative z ( $F_z$ ) and positive x directions ( $F_x$ ). As shown in Fig. 2b inset (attached video), beads in optical images showed darkened color after the DNA tether touched the CNT sidewall, suggesting that the beads were pulled up by the CNT to the position above the focal-plane (or the center of optical traps).

Next, we simultaneously moved two optical traps in the positive z direction to detach the hybrid DNA from the CNT.  $|F_z|$  gradually decreased when the DNA tether moved up until the optical trap centers return to the electrode plane (z=0), where the DNA tether remained in a straight line without bending upward or downward ( $F_z=0$ ). When pulling the DNA tether further up from the CNT,  $F_z$  started to increase again, but in the positive z direction, since the DNA molecule was still attached to the CNT and pulled the beads below the optical trap centers (or the focal plane), as shown in Fig. 2b inset where the beads that held the DNA tether appeared brighter. When we continued to pull the DNA tether up, both  $F_z$  and  $F_x$  abruptly dropped, suggesting the DNA tether was detached from the CNT surface.  $F_x$  on each bead is responsible for stretching the DNA tether in the lateral direction, whereas  $F_z$  corresponds to the binding force between the CNT and the hybrid DNA. Note that when we performed similar experiments with dsDNA tethers without ssDNA segments, no abrupt force drop was detected within our instrument detection limit

(Fig. S4), indicating that the abrupt force drop mainly results from the detachment of ssDNA segments from the CNT surface.

We further look into the detachment process of ssDNA-CNT interactions in detail. The top panel of Fig. 2c shows the positions of optical trap centers relative to the electrode plane in a 1second timeframe; the bottom panel displays the forces exerted on the bead by optical tweezers in the x (red) and z (blue) directions, respectively. When we slowly moved up the optical traps,  $F_z$ and  $F_x$  abruptly dropped  $0.7 \pm 0.1$  pN and  $0.8 \pm 0.2$  pN, respectively. More importantly, after the sudden force change, the bead no longer experienced forces in the axial direction when we slightly moved the DNA tether up and down, suggesting the DNA tether was indeed detached from the CNT surface. The binding force between ssDNA segments and the CNT was the combination of the forces in the axial direction from both left and right optical traps, distributing into three groups:  $1.2 \pm 0.5$  pN,  $3.3 \pm 0.5$  pN, and  $4.8 \pm 0.1$  pN and displaying a linear relationship (Fig. 3a). We also know that the length per base of ssDNA is about 0.5 nm,<sup>51</sup> which is smaller than the average diameter of CNTs (1.1 nm, Fig. 3b and 3c) used in our experiments. This allows 1 – 3 ssDNA bases to bind simultaneously to the CNT surface (Fig. 3d). Therefore, these distinctive groups of binding forces are likely due to the interactions between different lengths of ssDNA segments (or numbers of bases) and the CNT surface, where the binding force for a single base on the CNT surface is  $1.2 \pm 0.5$  pN. Since the interaction between the sugar-phosphate backbone of ssDNA and the CNT surface is too weak to be detected by our force sensor as demonstrated in our dsDNA-CNT experiments, the measured binding force is likely attributed to the interactions between a nitrogenous base and the hexagonal CNT sidewall. The standard deviation of the binding force may result from the interactions between different orientations/types of DNA bases and CNTs.<sup>27-</sup> 32, 52-57

Interestingly, the binding forces between ssDNA and CNTs measured in our optical trapping system are much smaller than those reported in previous studies by peeling ssDNA homopolymers from graphitic surfaces using an atomic force microscopy (AFM). 16, 58-60 Most of the AFM based studies were performed in a high loading rate regime or far-equilibrium regime, where the rupture force depends on the loading rate and is expected to be significantly larger than the equilibrium force. 16, 58-60 However, the loading rates used in our optical trapping system are 0.01~1.0 pN/s, which are four orders of magnitude lower than those used in previous AFM studies. 16, 58-60 More importantly, there is no obvious loading rate dependence observed in our measurements, suggesting that our measurements are performed in the near-equilibrium regime.<sup>61</sup> We also found that the measured binding force is smaller than the maximum adhesive force estimated from derivatives of smooth continuous energy functions in previous studies. 62, 63 In our experiments, external forces are discontinuous functions with a jump discontinuity at the displacement coordinate, leading to a jump discontinuous change in the complex geometry. As a result, the measured binding forces could be smaller than the maximum adhesive forces. Moreover, the contact zone between the curved CNT and orthogonally-aligned DNA molecule is very small and thus a limited number of atoms is expected to contribute the adhesion. In addition, the complicated geometry between the curved CNT and DNA molecule will influence the adhesive force between them.

Based on the measured equilibrium force, we calculated the binding free energy per base. For optical tweezers, the trapped beads display a Hookean response to the displacement relative to the center of an optical trap. The CNT-DNA bond and the force transducer (bead-DNA-bead tether) are either in the bound state (where a bond is formed between a CNT and DNA base) or in the unbound state (where the system fluctuates in the potential well of the force transducer). The

equilibrium force between the bound and unbound states of the system is given by  $f_{eq} = \sqrt{2k\Delta G}$ , where k is the stiffness of the optical traps, and  $\Delta G$  is the equilibrium free energy change between the bound and the unbound states.<sup>64</sup> In our measurements, the stiffness in the z direction is 0.013 pN/nm and the average binding force between a DNA base and a CNT is about 1.2 pN. The calculated equilibrium free energy change is  $\sim 0.34$  eV, which is in good agreement with theoretical simulations.<sup>27-36</sup>

To further elucidate the binding dynamics between CNTs and DNA molecules, we record the morphology changes of CNTs through 3D scanning photocurrent microscopy. As shown in Figure 4, the z position is the distance between optical trap centers and electrodes, where z = 0indicates that the optical trap centers and electrodes lie in the same plane. Initially, a CNT suspended between the two electrodes and bent slightly upward, a typical morphology for CNTs in aqueous media. When we pushed down a DNA tether in the perpendicular direction of the CNT (z = -800 nm), the CNT was dragged down as observed from its photocurrent image in the yz plane. When the DNA tether was moved up, the CNT was pulled up by the DNA tether until it detached from the CNT surface (z = 1200 nm). 3D scanning photocurrent measurements allow us to comprehensively monitor the morphology changes of a CNT, providing more information of CNT-DNA binding dynamics. We also noticed slight changes of photocurrent signals while DNA tether touched and detached from the CNT, which may be related to the electron transfer between them. More accurate measurements of CNT photocurrent changes, under different CNT-DNA interaction conditions, may be required to pin down the relationship between CNT photocurrent responses and the electrical coupling between CNTs and DNA molecules in future studies.

In conclusion, by combining dual-trap optical tweezers with 3D scanning photocurrent microscopy, we have designed an ultrasensitive CNT force sensor to investigate the mechanical

coupling between individual DNA molecules and CNTs at the single-molecule level in the near-equilibrium regime. The binding force and free energy between a single DNA base and a CNT are likely  $1.2\pm0.5$  pN and 0.34 eV, respectively. The integration of single molecule force spectroscopy with low-dimensional materials based nanoelectronics not only sheds light on the fundamental understanding of mechanical coupling between CNTs and DNA molecules, but also opens up new avenues for direct observation of intermolecular interface at the single-molecule level.

## Acknowledgments

This work was supported by the National Science Foundation (ECCS-1055852 and ECCS-1810088). Device Fabrication was conducted at the Center for Nanophase Materials Sciences, which is a DOE Office of Science User Facility.

## **Supporting information**

Experimental methods and materials describe: the device fabrication and CNTs synthesis, 3D scanning photocurrent microscopy, dual-trap optical tweezers, microfluidic chamber assembly, DNA preparation, creating ssDNA-dsDNA hybrids, video based bead position tracking and force determination, comparison of forces inferred from PSD and video image, and interaction between dsDNA and CNT.

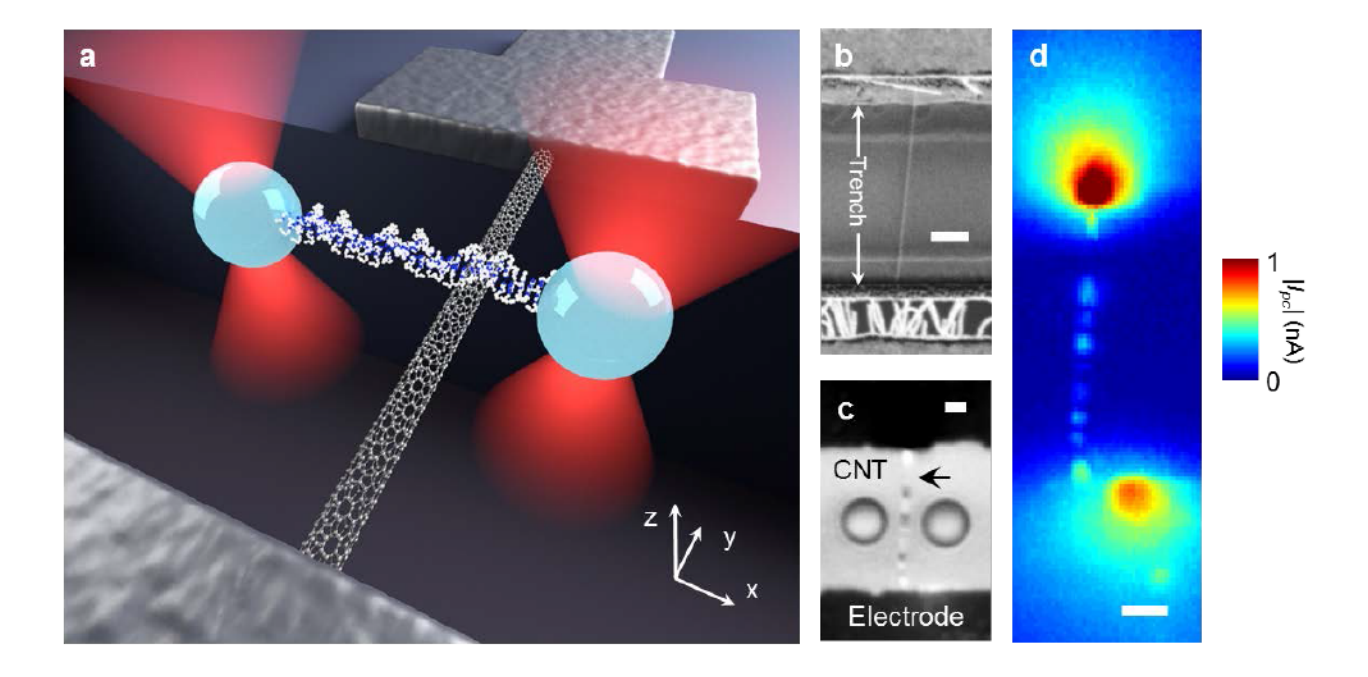
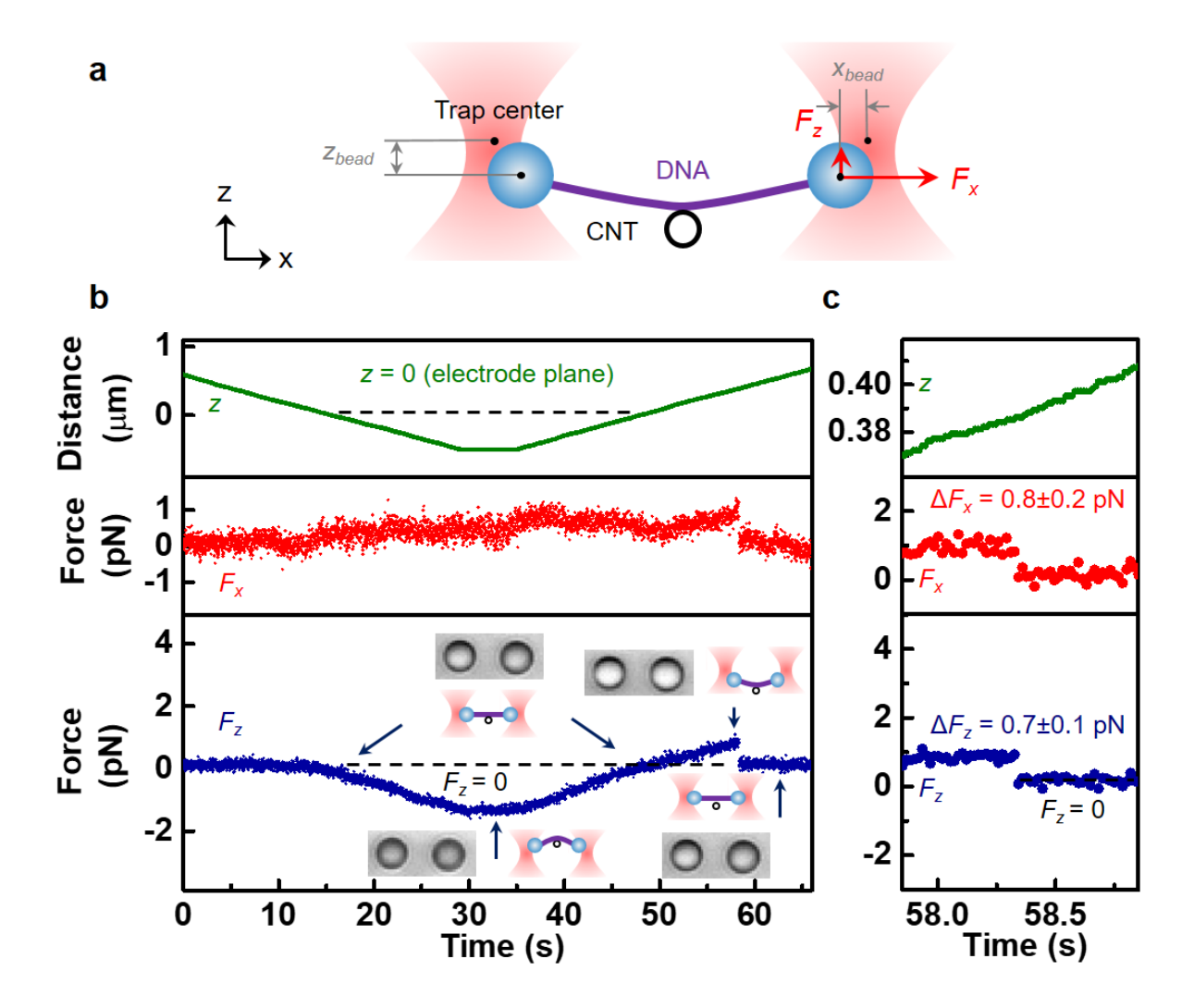
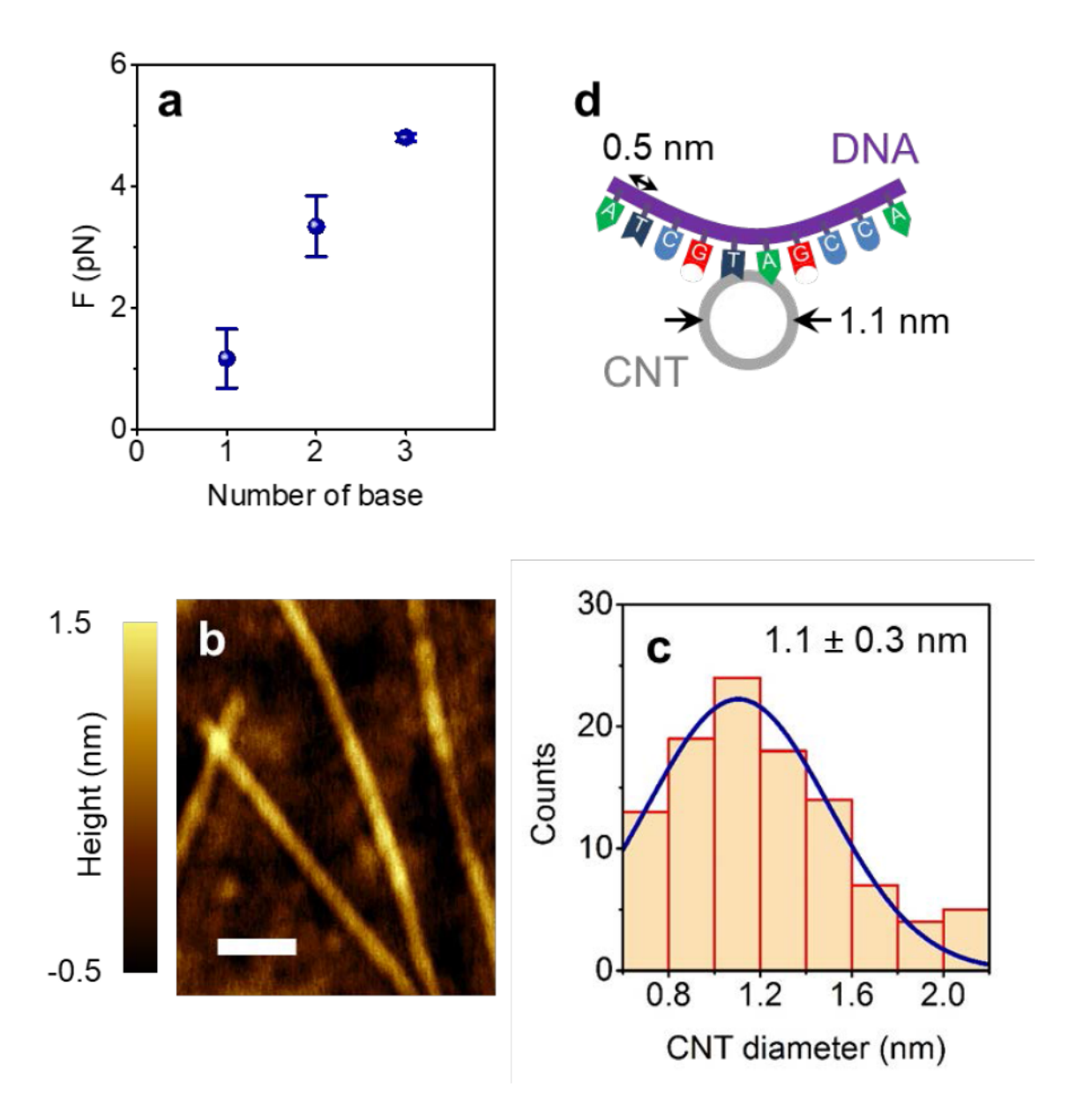


Figure 1. (a) Schematic of a CNT transistor combined with dual-trap optical tweezers. A suspended CNT was synthesized across a 5 μm wide, 4 μm deep trench on a 170 μm thick fused silica substrate. The DNA was controlled by dual-trap optical tweezers via polystyrene beads and placed in the perpendicular direction to the CNT. The coordinates are defined in the lower right corner. (b) Scanning electron microscope image of a typical CNT transistor. (c) Overlap of optical and photocurrent images of a CNT transistor. The relative position of a DNA tether to the CNT can thus be identified. (d) Scanning photocurrent image of a CNT transistor in the *xy* plane. The scale bars in b-d are 1 μm.



**Figure 2.** (a) Experimental geometry of a DNA tether attached to a CNT in the xz plane. Optical traps applied forces to the beads in both lateral (x) and axial (z) directions. (b) CNT-DNA interactions as a function of time. The green curve shows the distance between the optical trap centers and electrodes in the z direction. The red and blue curves represent forces applied to the right bead by an optical trap in the x and z directions, respectively. Inset: optical images of beads (in the xy plane) and corresponding schemes (in the xz plane) showing the relative positions between the CNT (black circle) and the DNA tether (purple line). (c) Optical trap center position in the z direction (green) and force changes in the x (red) and z (blue) directions with standard deviations when DNA was detached from the CNT.



**Figure 3. (a)** Average binding force with standard deviation for different numbers of DNA bases that bind to a CNT. (b) AFM image of CNTs on a fused silica substrate. The scale bar is 100 nm. (c) Histogram of CNT diameter distribution. The CNTs show an average height of  $1.1 \pm 0.3$  nm. (d) Schematics of ssDNA bases binding on CNTs.

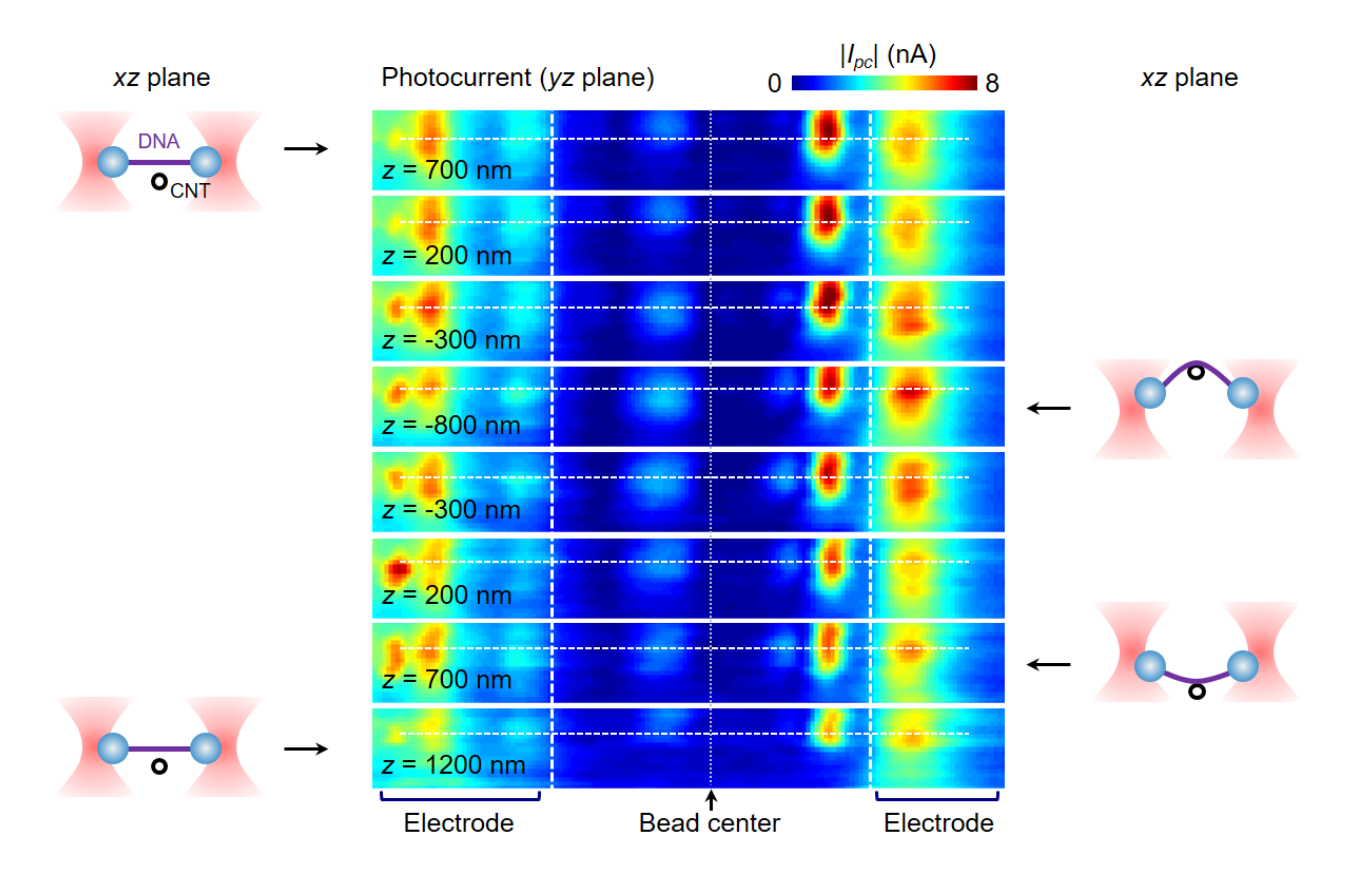


**Figure 4.** Morphology change of a CNT during its interaction with a DNA tether monitored by 3D scanning photocurrent microscopy in the yz plane. The horizontal dashed white lines mark the positions of the electrode plane. The distance between two electrodes is 7  $\mu$ m. The schematics show the relative positions between the CNT and the DNA tether in the xz plane.

## **REFERENCES AND NOTES**

- 1. Zheng, M.; Jagota, A.; Strano, M. S.; Santos, A. P.; Barone, P.; Chou, S. G.; Diner, B. A.; Dresselhaus, M. S.; McLean, R. S.; Onoa, G. B.; Samsonidze, G. G.; Semke, E. D.; Usrey, M.; Walls, D. J. *Science* **2003**, 302, (5650), 1545-1548.
- 2. Zheng, M.; Jagota, A.; Semke, E. D.; Diner, B. A.; Mclean, R. S.; Lustig, S. R.; Richardson, R. E.; Tassi, N. G. *Nat Mater* **2003**, 2, (5), 338-342.
- 3. Hernandez, Y.; Nicolosi, V.; Lotya, M.; Blighe, F. M.; Sun, Z.; De, S.; McGovern, I. T.; Holland, B.; Byrne, M.; Gun'Ko, Y. K.; Boland, J. J.; Niraj, P.; Duesberg, G.; Krishnamurthy, S.; Goodhue, R.; Hutchison, J.; Scardaci, V.; Ferrari, A. C.; Coleman, J. N. *Nat Nanotechnol* **2008**, 3, (9), 563-8.
- 4. Coleman, J. N.; Lotya, M.; O'Neill, A.; Bergin, S. D.; King, P. J.; Khan, U.; Young, K.; Gaucher, A.; De, S.; Smith, R. J.; Shvets, I. V.; Arora, S. K.; Stanton, G.; Kim, H. Y.; Lee, K.; Kim, G. T.; Duesberg, G. S.; Hallam, T.; Boland, J. J.; Wang, J. J.; Donegan, J. F.; Grunlan, J. C.; Moriarty, G.; Shmeliov, A.; Nicholls, R. J.; Perkins, J. M.; Grieveson, E. M.; Theuwissen, K.; McComb, D. W.; Nellist, P. D.; Nicolosi, V. *Science* **2011**, 331, (6017), 568-571.
- 5. Wang, R.; Shi, M. J.; Brewer, B.; Yang, L. J.; Zhang, Y. C.; Webb, D. J.; Li, D. Y.; Xu, Y. Q. *Nano Letters* **2018**, 18, (9), 5702-5708.
- 6. Podzorov, V. *Nat Mater* **2010,** 9, (8), 616-616.
- 7. Fischer, R. A.; Zhang, Y.; Risner, M. L.; Li, D.; Xu, Y.; Sappington, R. M. *Advanced Healthcare Materials* **2018**, 1701290.
- 8. Kitko, K. E.; Hong, T.; Lazarenko, R. M.; Ying, D.; Xu, Y. Q.; Zhang, Q. *Nat Commun* **2018,** 9, 796.
- 9. Hong, T.; Lazarenko, R. M.; Colvin, D. C.; Flores, R. L.; Zhang, Q.; Xu, Y.-Q. *The Journal of Physical Chemistry C* **2012**, 116, (30), 16319-16324.
- 10. Qiao, J. B.; Hong, T.; Triana, T. S.; Guo, H. L.; Chung, D. H.; Xu, Y. Q. *Rsc Advances* **2013,** 3, (14), 4544-4551.
- 11. Harvey, J. D.; Jena, P. V.; Baker, H. A.; Zerze, G. H.; Williams, R. M.; Galassi, T. V.; Roxbury, D.; Mittal, J.; Heller, D. A. *Nat Biomed Eng* **2017**, 1, (4).
- 12. Hof, F.; Trembleau, L.; Ullrich, E. C.; Rebek, J. *Angew Chem Int Edit* **2003,** 42, (27), 3150-3153.
- 13. Steuber, H.; Heine, A.; Klebe, G. J Mol Biol **2007**, 368, (3), 618-638.
- 14. Paliwal, S.; Geib, S.; Wilcox, C. S. *Journal of the American Chemical Society* **1994,** 116, (10), 4497-4498.
- 15. Carver, F. J.; Hunter, C. A.; Seward, E. M. *Chem Commun* **1998**, (7), 775-776.
- 16. Manohar, S.; Mantz, A. R.; Bancroft, K. E.; Hui, C. Y.; Jagota, A.; Vezenov, D. V. *Nano Letters* **2008**, 8, (12), 4365-4372.
- 17. Piao, Y. M.; Meany, B.; Powell, L. R.; Valley, N.; Kwon, H.; Schatz, G. C.; Wang, Y. H. *Nat Chem* **2013,** 5, (10), 840-845.
- 18. Heller, D. A.; Jeng, E. S.; Yeung, T. K.; Martinez, B. M.; Moll, A. E.; Gastala, J. B.; Strano, M. S. *Science* **2006**, 311, (5760), 508-511.
- 19. Zhong, Z. H.; Gabor, N. M.; Sharping, J. E.; Gaeta, A. L.; McEuen, P. L. *Nature Nanotechnology* **2008,** 3, (4), 201-205.
- 20. Kim, P.; Shi, L.; Majumdar, A.; McEuen, P. L. *Physical Review Letters* **2001**, 87, (21).

- 21. Minot, E. D.; Yaish, Y.; Sazonova, V.; Park, J. Y.; Brink, M.; McEuen, P. L. *Physical Review Letters* **2003**, 90, (15).
- 22. Sorgenfrei, S.; Chiu, C. Y.; Gonzalez, R. L.; Yu, Y. J.; Kim, P.; Nuckolls, C.; Shepard, K. L. *Nature Nanotechnology* **2011,** 6, (2), 125-131.
- 23. Choi, Y. K.; Moody, I. S.; Sims, P. C.; Hunt, S. R.; Corso, B. L.; Perez, I.; Weiss, G. A.; Collins, P. G. *Science* **2012**, 335, (6066), 319-324.
- 24. Neuman, K. C.; Block, S. M. Rev Sci Instrum **2004**, 75, (9), 2787-2809.
- 25. Neuman, K. C.; Nagy, A. Nature Methods 2008, 5, 491.
- 26. Abbondanzieri, E. A.; Greenleaf, W. J.; Shaevitz, J. W.; Landick, R.; Block, S. M. *Nature* **2005**, 438, (7067), 460-465.
- 27. Das, A.; Sood, A. K.; Maiti, P. K.; Das, M.; Varadarajan, R.; Rao, C. N. R. *Chemical Physics Letters* **2008**, 453, (4), 266-273.
- 28. Lv, W. Chemical Physics Letters **2011**, 514, (4), 311-316.
- 29. Johnson Robert, R.; Johnson, A. T. C.; Klein Michael, L. Small **2009**, 6, (1), 31-34.
- 30. Chehel Amirani, M.; Tang, T.; Cuervo, J. *Physica E: Low-dimensional Systems and Nanostructures* **2013**, 54, 65-71.
- 31. Wang, Y. The journal of physical chemistry. C, Nanomaterials and interfaces **2008**, 112, (37), 14297-14305.
- 32. Shtogun, Y. V.; Woods, L. M.; Dovbeshko, G. I. *The Journal of Physical Chemistry C* **2007**, 111, (49), 18174-18181.
- 33. Gowtham, S.; Scheicher, R. H.; Pandey, R.; Karna, S. P.; Ahuja, R. *Nanotechnology* **2008**, 19, (12), 125701.
- 34. Frischknecht, A. L.; Martin, M. G. *The Journal of Physical Chemistry C* **2008,** 112, (16), 6271-6278.
- 35. Yamazaki, T.; Fenniri, H. The Journal of Physical Chemistry C 2012, 116, (28), 15087-15092.
- 36. Umadevi, D.; Sastry, G. N. *The Journal of Physical Chemistry Letters* **2011,** 2, (13), 1572-1576.
- 37. Xu, Y. Q.; Barnard, A.; McEuen, P. L. *Nano Letters* **2009**, 9, (4), 1609-1614.
- 38. Avouris, P.; Freitag, M.; Perebeinos, V. *Nat Photonics* **2008**, 2, (6), 341-350.
- 39. Sun, D.; Aivazian, G.; Jones, A. M.; Ross, J. S.; Yao, W.; Cobden, D.; Xu, X. D. *Nature Nanotechnology* **2012**, **7**, (2), 114-118.
- 40. Rosenblatt, S.; Yaish, Y.; Park, J.; Gore, J.; Sazonova, V.; McEuen, P. L. *Nano Letters* **2002**, 2, (8), 869-872.
- 41. Kruger, M.; Buitelaar, M. R.; Nussbaumer, T.; Schonenberger, C.; Forro, L. *Appl Phys Lett* **2001**, 78, (9), 1291-1293.
- 42. Moffitt, J. R.; Chemla, Y. R.; Izhaky, D.; Bustamante, C. *Proceedings of the National Academy of Sciences of the United States of America* **2006**, 103, (24), 9006-9011.
- 43. Tu, X. M.; Manohar, S.; Jagota, A.; Zheng, M. *Nature* **2009**, 460, (7252), 250-253.
- 44. Johnson, R. R.; Kohlmeyer, A.; Johnson, A. T. C.; Klein, M. L. *Nano Letters* **2009**, 9, (2), 537-541.
- 45. Johnson, R. R.; Johnson, A. T. C.; Klein, M. L. *Nano Letters* **2008**, 8, (1), 69-75.
- 46. Zhao, X.; Johnson, J. K. *Journal of the American Chemical Society* **2007,** 129, (34), 10438-10445.
- 47. Smith, S. B.; Cui, Y. J.; Bustamante, C. Science **1996**, 271, (5250), 795-799.

- 48. Candelli, A.; Hoekstra, T. P.; Farge, G.; Gross, P.; Peterman, E. J. G.; Wuite, G. J. L. *Biopolymers* **2013**, 99, (9), 611-620.
- 49. King, G. A.; Gross, P.; Bockelmann, U.; Modesti, M.; Wuite, G. J. L.; Peterman, E. J. G. *Proceedings of the National Academy of Sciences of the United States of America* **2013,** 110, (10), 3859-3864.
- 50. Crocker, J. C.; Grier, D. G. *J Colloid Interf Sci* **1996,** 179, (1), 298-310.
- 51. Bockelmann, U.; Essevaz-Roulet, B.; Heslot, F. *Phys Rev E* **1998,** 58, (2), 2386-2394.
- 52. Meng, S.; Wang, W. L.; Maragakis, P.; Kaxiras, E. *Nano Letters* **2007,** 7, (8), 2312-2316.
- 53. Wang, H. M.; Ceulemans, A. *Phys Rev B* **2009**, 79, (19).
- 54. Akdim, B.; Pachter, R.; Day, P. N.; Kim, S. S.; Naik, R. R. *Nanotechnology* **2012,** 23, (16).
- 55. Ramraj, A.; Hillier, I. H.; Vincent, M. A.; Burton, N. A. *Chemical Physics Letters* **2010**, 484, (4-6), 295-298.
- 56. Stepanian, S. G.; Karachevtsev, M. V.; Glamazda, A. Y.; Karachevtsev, V. A.; Adamowicz, L. *Chemical Physics Letters* **2008**, 459, (1-6), 153-158.
- 57. Shukla, M. K.; Dubey, M.; Zakar, E.; Namburu, R.; Czyznikowska, Z.; Leszczynski, J. *Chemical Physics Letters* **2009**, 480, (4-6), 269-272.
- 58. Zhang, Y. H.; Liu, C. J.; Shi, W. Q.; Wang, Z. Q.; Dai, L. M.; Zhang, X. *Langmuir* **2007**, 23, (15), 7911-7915.
- 59. Iliafar, S.; Wagner, K.; Manohar, S.; Jagota, A.; Vezenov, D. *J Phys Chem C* **2012,** 116, (26), 13896-13903.
- 60. Iliafar, S.; Mittal, J.; Vezenov, D.; Jagota, A. *Journal of the American Chemical Society* **2014,** 136, (37), 12947-12957.
- 61. Merkel, R.; Nassoy, P.; Leung, A.; Ritchie, K.; Evans, E. *Nature* **1999**, 397, 50.
- 62. Lechner, C.; Sax, A. F. The Journal of Physical Chemistry C 2014, 118, (36), 20970-20981.
- 63. Lechner, C.; Sax, A. F. Applied Surface Science **2017**, 420, 606-617.
- 64. Friddle, R. W.; Noy, A.; De Yoreo, J. J. *Proceedings of the National Academy of Sciences* **2012**, 109, (34), 13573-13578.